Acta Cryst. (1997). D**53**, 438–447

Different Tools to Study Interaction Potentials in γ-Crystallin Solutions: Relevance to Crystal Growth

F. BONNETÉ,[a] M. MALFOIS,[a] S. FINET,[a] A. TARDIEU,[a] S. LAFONT[b] AND S. VEESLER[b]

[a]*Laboratoire de Minéralogie Cristallographie Paris, UA 09, CNRS, Universités Paris VI, Paris VII Tour 16, Case 115, 4 place Jussieu, 75252 Paris CEDEX 05, France, and* [b]*Centre de Recherche sur les Mécanismes de la Croissance Cristalline, CNRS, Campus de Luminy, Case 913, 13288 Marseille CEDEX 09, France. E-mail: tardieu@lmcp.jussieu.fr*

(*Received 18 November 1996; accepted 31 January 1997*)

Abstract

Osmotic pressure, small-angle X-ray scattering and quasi-elastic light scattering were used to study the medium-range interaction potentials between macromolecules in solution. These potentials determine macromolecular crystallization. Calf eye lens γ-crystallins were used as a model system with the charge, and therefore the interactions, varied with pH. The second virial coefficient was determined under the same conditions with each of the three techniques. Osmotic pressure and quasi-elastic light scattering can be used conveniently in the laboratory to rapidly test the type of interactions (either attractive or repulsive) present in the solution. The measurement is direct with osmotic pressure, whereas with quasi-elastic light scattering, the directly measured coefficient is a combination of thermodynamic and hydrodynamic terms. X-rays, which require more sophisticated equipment such as synchrotron radiation facilities, can provide more detailed information on the interparticle potentials when models are used. At low ionic strength, two potentials were found necessary to account for the temperature and pH phase diagram as a function of protein concentration. The first potential is the van der Waals attractive potential that was previously shown to account for the fluid–fluid phase separation at low temperature. The second potential is an electrostatic coulombic repulsive potential which is a function of the protein charge and thus of the pH. The interaction trail could be followed at protein concentrations as low as 10 mg ml^{-1}. The results as a whole are expected to be valid for all compact low molecular weight proteins at low ionic strength.

1. Introduction

The medium-range non-specific interactions between biological macromolecules in solution include electrostatic contributions, van der Waals attractive interactions, and more ill-defined forces like hydration and hydrophobic effects (Israelachvili, 1994). These interactions or interaction potentials govern macroscopic properties such as solubility, transparency (Delaye & Tardieu, 1983; Tardieu & Delaye, 1988; Vérétout, Delaye & Tardieu 1989), viscosity and osmotic pressure (Parsegian, Rand, Fuller & Rau, 1986; Vérétout & Tardieu, 1989; Haynes, Tamura, Korfer, Blanch & Prausnitz, 1992). At the same time, they are relevant to understanding macromolecular phase diagrams including the process of phase separation (Thomson, Schurtenberger, Thurston & Benedek 1987; Taratuta, Holschbach, Thurston, Blankschtein & Benedek, 1990; Belloni, 1993; Malfois, Bonneté, Belloni & Tardieu, 1996) and the onset of macromolecular crystallization (Muschol & Rosenberger, 1995; Ducruix, Guilloteau, Riès-Kautt & Tardieu, 1996).

Three approaches, osmotic pressure (OP), small-angle X-ray scattering (SAXS), and quasi-elastic light scattering (QELS), may help us to study macromolecules in solution. In the absence of interactions, OP measures a number average molecular weight and SAXS a weight average molecular weight. SAXS measures a radius of gyration and QELS measures a diffusion coefficient related to the hydrodynamic radius. As far as interactions are concerned, attractive or repulsive regimes can be distinguished from the sign of the second virial coefficient measured directly by OP (Eisenberg, 1976), or measured in combination with hydrodynamic coefficients by QELS (Pecora, 1985). The shape of the SAXS curves is related to both the type (attractive or repulsive) and the shape of the interaction potentials (Tardieu, 1994). An approach combining SAXS, OP measurements and interaction model analysis was initially developed to study concentrated solutions and analyze the interactions relevant to the optical properties of the lens (Vérétout *et al.*, 1989; Tardieu, Vérétout, Krop & Slingsby, 1992). Later on, SAXS experiments as a function of salt concentration on concentrated lysozyme solutions in undersaturated conditions prior to crystallogenesis, demonstrated that crystallization involves attractive potentials. In addition, experiments performed with an anion series showed that the strength of the attraction was correlated to the displacement of the solubility curves, according to the reverse order of the Hofmeister series (Ducruix *et al.*, 1996). At the same time, and in part thanks to recent technological improvements, most studies devoted to study crystal nucleation and growth make use of light-

scattering techniques, either static (SLS) or QELS. They were initially used as a tool to detect, in under and supersaturated solutions, the evolution of polydispersity or the formation of high molecular weight species, that could indicate the onset of nucleation (Kam, Shore & Feher, 1978; Mikol, Hirsch & Giegé, 1990; Georgalis, Zouni & Saenger, 1992; Zulauf & D'Arcy, 1992; Malkin & McPherson, 1994; Veesler, Marcq, Lafont, Astier & Boistelle, 1994). Then, SLS and QELS also started to be used to study protein interactions, and their variations in crystallizing conditions (Skouri, Munch, Lorber, Giegé, & Candau, 1992; Eberstein, Georgalis & Saenger, 1994; George & Wilson, 1994; Muschol & Rosenberger, 1995; Lafont, Veesler, Astier & Boistelle, 1997; Veesler, Lafont, Marcq, Astier & Boistelle, 1996).

With the extension of the scientific interest from nucleation in supersaturated solutions to interactions in undersaturated solutions, it seemed to us worthwhile to reinvestigate the advantages and drawbacks of the three techniques, OP, SAXS and QELS. The comparison is, however, difficult to make from the data in the literature, since the availability of the equipment is quite different: QELS and OP are commercially available for laboratory use, although membrane osmometers are less widely distributed, whereas SAXS requires a synchrotron radiation facility equipped with a small-angle camera. Moreover, the published data have been obtained on different systems, examined at different concentrations and under different physico-chemical conditions. For instance, most SAXS studies were performed with concentrated solutions and QELS studies with dilute ones. The experiments presented here were, therefore, specially designed to allow comparison of the techniques. Total γ-crystallins extracted from calf lenses were used as a model system. These proteins are coded by a multigene family with a high level of identity between members. They are globular proteins with 173–174 amino acids and a molecular weight, M, of about 21 kDa with similar three-dimensional structures (White, Driessen, Slingsby, Moss & Lindley, 1989; Wistow *et al.*, 1983). They are monomers in solution and their attractive behaviour in physiological conditions had already been analysed with OP and SAXS in relation to the optical properties of the lens (Vérétout & Tardieu, 1989; Tardieu *et al.*, 1992; Malfois, 1995). In particular, the cold cataract opacity which develops in the central part of young mammalian lenses at low temperature, known to result from a phase separation of the γ-crystallins, had been shown recently to result from a short-range attractive potential (Lomakin, Asherie & Benedek, 1996; Malfois *et al.*, 1996). The γ-crystallins were, in addition, especially suited for our present purpose since their charge, and thus the interaction potentials, could be varied in a simple way by changing the pH of the solution at low ionic strength. Moreover, because of the γ-crystallin molecular weight of 21 kDa, the three types of experiment could be performed with the same samples. The interest in pH variation has been demonstrated for lysozyme by Riès-Kautt and Ducruix (private communication).

2. Theory

2.1. *Interaction potentials*

The behaviour of macromolecules in aqueous solutions is governed by the interparticle interactions as well as by the particle–solvent and particle–ion (or small solute) interactions (Hansen & McDonald, 1986; Israelachvili, 1994). As a first approximation to the description of the behavior of biological macromolecules, only the interaction potentials between macromolecules are considered (Belloni, 1991). The solvent is treated as a medium of uniform dielectric constant and the ions as point charges (in a second step, some chemistry may be introduced if necessary). The weak intermacromolecular forces include a number of contributions which, with caution, can be combined. In the colloid field, combinations used currently include hard-core, repulsive electrostatic coulombic and attractive van der Waals interactions. At very short distances, a few Å, the hard-sphere or hard-core potential is the expression of the fact that macromolecules cannot interpenetrate. The electrostatic coulombic forces result from the effective charge of the macromolecule and vary from a few Å to nm. With monodisperse solutions of identical particles the coulombic pair potential is, therefore, repulsive. With proteins in aqueous buffer, the potential is expected to vary as a function of pH since the overall charge of the macromolecule is a function of pH. In addition, the potential is expected to be screened with increasing ionic strength. van der Waals attractive forces are expected to be pretty much the same from one protein to another, as long as the protein compactness remains the same. These attractive interactions vary as a function of $1/kT$. The van der Waals potential has been shown to be sufficient to account for γ-crystallin phase separation as a function of temperature at pH 7 (Malfois, 1995; Malfois *et al.*, 1996).

2.2. *Osmotic pressure and virial coefficients*

In an osmotic pressure experiment, the solvent and the protein solution are equilibrated on each side of a semipermeable membrane (Eisenberg, 1976; Parsegian *et al.*, 1986). When the protein concentration is increased in one compartment, a solvent flux is observed through the membrane towards this compartment, until the excess pressure induced by the addition of macromolecule is compensated, *e.g.* by the hydrostatic pressure increase due to a δh difference in the solvent level in the two compartments. The osmotic pressure Π, expressed in 10^{-5} N cm^{-2} is written,

$$\Pi = \rho g \delta h, \qquad (1)$$

where ρ (g cm^{-3}) is the solution density, $g = 981$ cm s^{-2} is the gravitation constant and δh is expressed in cm.

Closely parallel to the properties of gas systems, the osmotic pressure Π can be expressed as a function of the number of particles per unit volume of solution, ρ_n (mol cm^{-3}), and the interactions between them described by the second and higher virial coefficients B_i,

$$\Pi/\rho_n kT = 1 + B_2\rho_n + B_3\rho_n^2 + \ldots, \quad (2)$$

where k is the Boltzmann constant, 1.38×10^{-23} J K^{-1}, and T the absolute temperature. Osmotic pressure is a colligative method which counts the number of particles. In practice, ρ_n is converted into macromolecular concentration c (g cm^{-3}) using $\rho_n/N_A = c/M$ where M is the molecular weight in Da and N_A Avogadro's number to yield,

$$\Pi/cRT = 1/M + A_2c + A_3c^2 + \ldots, \quad (3)$$

where R is the gas constant, 8.31 J K^{-1} mol^{-1}. Thus, $A_2 = B_2N_A/M^2$ (mol cm^3 g^{-2}). When the concentration is known, the first virial coefficient provides us with the protein mass. The sign of the second virial coefficient, A_2 or B_2, is indicative of the type of interactions. It is negative with attractive interactions and positive with repulsive interactions

2.3. *Small-angle X-ray scattering and structure factors*

The intensity scattered by one particle as a function of the scattering vector **s** (where $s = 2\sin\theta/\lambda$ and 2θ is the scattering angle), usually called the particle form factor, is the Fourier transform of the spherically averaged auto-correlation function of the electron-density contrast associated with the particle. When the solution is ideal, *i.e.* in the absence of interactions, the total scattering, $I(0, s)$, is the sum of the scattering of the individual particles (Luzzati & Tardieu, 1980). With solutions of monodisperse spherical particles, and in the presence of interactions, departure from ideality may be accounted for simply by a multiplying factor or interference term, $S(c, s)$, which is a function of the scattering angle,

$$I(c, s) = I(c, 0)S(c, s). \quad (4)$$

$S(c, s)$ is usually called the solution structure factor. The equation can still be considered valid, yet within a smaller s range, with quasi-spherical particles and/or polydisperse particles (Tardieu, 1994). To calculate the experimental structure factors, a form factor is needed. The form factor was obtained from the 10 mg ml^{-1} concentration curve recorded at the isoelectric point, by extrapolating towards the origin the linear part of the Guinier plot (Guinier & Fournet, 1955). The linear part of the plot is obtained outside the low-angle region where the interactions play a part.

Since the solution can be described mathematically as the convolution product of a particle shape and a particle distribution (*i.e.* a set of delta functions placed at the particle centers), $S(c, s)$ is the Fourier transform of the spherically averaged auto-correlation function $g(r)$ of the particle distribution.

$$S(c, s) = 1 + (N/V)\int 4\pi r^2[g(r) - 1](\sin 2\pi rs/2\pi rs)\mathrm{d}r, \quad (5)$$

where (N/V) is the number of particles per unit volume and c is the particle concentration (g cm^{-3}). The structure factor at the origin, $S(c, 0)$ is proportional to compressibility. With repulsive interactions, the particles are evenly distributed and $S(c, 0)$ is lower than 1. With attractive interactions, fluctuations in the particle distribution are observed which lead to a $S(c, 0)$ value larger than 1. To calculate a theoretical structure factor from macromolecular interactions, the pair particle potential taken as a model is written, either attractive or repulsive, from which a particle distribution $g(r)$ at equilibrium is inferred. The structure factor $S(c, s)$, and/or macroscopic properties and thermodynamic variables, are then calculated from the Fourier transform and integrals of the pair distribution function $g(r)$ (Belloni, 1991, 1993). The numerical method is iterative. The hypernetted chain integral equation is solved for a fluid of hard spheres with attractive and repulsive Yukawa tails (Belloni, 1993), which means that the potentials are described by three parameters, particle diameter, potential range and potential depth.

In the present study, a minimum of two potentials, a repulsive one and an attractive one, were needed to account for the experimental data. It had been shown in a previous study that the γ-crystallin phase separation could be accounted for by an attractive van der Waals potential with a hard core, which is a function of three parameters: hard core diameter, and potential range and depth from which the Hamaker constant, usually adopted to describe the strength of the van der Waals forces (Israelachvili, 1994), can be calculated. The particle diameter was shown to be equal to the diameter of the sphere occupying the γ-crystallin dry volume, *i.e.* 36 Å, and the attractive potential was shown to be short range, around 3 Å. These values were, therefore, fixed in the present study and assumed invariant with pH and ionic strength. The Hamaker constant calculated to account for the phase separation was of the order of $3kT$, in good agreement with the value calculated for proteins in aqueous solvents from refractive index and dielectric constant (Israelachvili, 1994). Since, however, this fitted Hamaker constant was found to vary slightly as a function of protein concentration, it was left as a variable in the present study. The variation of the structure factors as a function of pH was accounted for by the addition of a coulombic repulsive potential. Such a potential depends upon an effective particle charge which included counterion contributions, and upon Debye length. The Debye length is known when the ionic strength is known. Therefore, the fitting parameters are

the Hamaker constant and the particle charge (Malfois, 1995; Malfois *et al.*, 1996).

2.4. *Quasi-elastic light scattering: the contribution of dynamic coefficients*

QELS measurements analyse the scattering intensity fluctuations, which are related to the motions of the macromolecular solute. The time dependence of the fluctuations are analysed with a correlator, so that QELS experiments measure a photon correlation function (PCF). With monodisperse solutions of non-interacting particles, the PCF decay as a function of time is mono exponential. The PCF decay may become rather complicated in the presence of interacting and/or polydisperse particles (Pecora, 1985).

The initial decay of the PCF is determined by particle motions taking place at short times. In this case the PCF is most conveniently analysed in terms of a cumulant expansion (Koppel, 1972),

$$\mathrm{Ln(PCF)}^{1/2} = \sum_n K_n(-\tau)^n/n!, \tag{6}$$

where τ is the correlation decay time and K_n is the nth cumulant. The first cumulant K_1 defines an effective diffusion coefficient governing the initial decay of the PCF,

$$K_1 = D_{\mathrm{eff}}\mathbf{q}^2, \tag{7}$$

where $\mathbf{q} = (4\pi n/\lambda)\sin(\theta/2)$ is the scattering vector, θ the scattering angle and n the refractive index (note that with X-rays the angle θ is called 2θ and that the light-scattering $\mathbf{q}$ vector is equal to the X-ray scattering vector $\mathbf{s}$ multiply by 2π). The higher cumulants characterize the subsequent departure from exponential behavior. With non-interacting particles,

$$\begin{aligned} K_1 &= D_0\mathbf{q}^2, \\ \text{and } K_n &= 0 \text{ for } n \geq 2, \end{aligned} \tag{8}$$

where D_0 is the free particle diffusion coefficient. D_0 is equal to $kT/6\pi\eta R_h$, where η is the solvent viscosity and R_h the hydrodynamic radius. At short times and $\mathbf{q} \to 0$, D_{eff} is identified to the mutual diffusion coefficient D_m. D_m is governed by direct thermodynamic and indirect hydrodynamic interactions. The expression for D_m is,

$$D_m = D_0[1 + H(0)]/S(0), \tag{9}$$

where $S(0)$ is the $\mathbf{q} \to 0$ limit of the structure factor [note that with X-rays, the same structure factor at the origin is called $S(c, 0)$] and $H(0)$ is the $q \to 0$ limit of the hydrodynamic term (because of the coupling between particle motions transmitted indirectly by the liquid motions that they induce).

3. Materials and methods

3.1. *Osmotic pressure measurements*

The osmotic pressure experiments were performed at the Laboratoire de Minéralogie Cristallographie, Paris, with a KNAUER membrane osmometer, using Amicon YM 10 membranes. The osmometer comprises a lower part (solvent cell) and an upper part (solution cell) separated by the semi-permeable membrane, 12 mm in diameter. The calibration is made against a known hydrostatic pressure. The system is thermostated. The upper cell is filled with the solution to be measured. A piezo-electric captor measures the pressure difference, δh (equation 1), between the two solutions after equilibration. With low ionic strength aqueous buffers of density close to 1, $\delta h = 1$ mm corresponds to an OP of 98.1×10^{-5} N cm^{-2}.

The upper cell was first equilibrated with solvent. Then a sample concentration series was prepared with the same stock solution, and the least concentrated sample was measured first. Measurements were made at 298 K. About 40 µl were needed for each measurement, and each point was repeated three times. The time needed for equilibration was of the order of 5–15 min.

3.2. *X-ray experiments*

The experiments were carried out using the small-angle instrument D24 (Depautex *et al.*, 1987) at the Laboratory for Synchrotron Radiation, LURE (Orsay, France) where measurements can be performed in a short time, typically in a few minutes, with point collimation and monochromatic radiation. The X-ray beam was monochromatized ($\lambda = 1.488$ Å, K edge of Ni) and focussed with a bent germanium crystal. The X-ray beam had a full-width cross section of about 0.5×1.0 mm at the detector level. Parasitic scattering was eliminated using pairs of tantalum slits, vertical and horizontal. Data were collected using a linear position-sensitive detector with a delay line readout positioned vertically. In the γ-crystallin experiments, the sample-to-detector distance was 1232 mm. The angular increment ds/channel was, therefore, 2.370×10^{-4} Å^{-1}. The experiments made use of a specially designed quartz cell that could be filled and rinsed *in situ* (kindly provided by P. Vachette). Average exposure times were about 5 min for samples and buffers. The intensity curves were subtracted for background and normalized for concentration and direct beam intensity, but otherwise uncorrected. $I_{\mathrm{exp}}(c,s)$ were scaled on a relative value according to Luzzati & Tardieu (1980),

$$I(c,s) = I_{\mathrm{exp}}(c,s)/E_0c, \tag{10}$$

where E_0 is proportional to the photon number of the incident beam (measured by reference to a carbon sample).

3.3. *Light-scattering measurements*

QELS experiments were performed at the Centre de Recherche sur les Mécanismes de Croissance Cristalline (Marseille) on a SEM 633 light-scattering apparatus (Sematech, Nice) with an argon ion laser running at a power ranging from 50 to 500 mW and operating at 514.5 nm (Spectra-Physics 2017). The measurements were performed at 90° and were processed through a multi-τ correlator (UNICOR) with different sample times between 0.1 and 1 µs. Before each measurement, the samples were centrifuged, filtered through a 0.5 µm Millex LCR single-use membrane (Millipore) and introduced according to the sample quantities in a cylindrical glass cuvette with a diameter of either 12 or 8 mm; the sample volume was about 300 and 80 µl, respectively; solvent density and viscosity were taken equal to the water values *i.e.* 1.

Diffusion coefficients were computed by the method of cumulants and the expension was carried out either at the first or the second order. In both cases the first cumulant was extracted. At each concentration, experiments were performed at different sampling times ranging from 0.1 to 1 µs. Diffusion coefficients were plotted *versus* sampling time. The intercept at $\tau = 0$ gave a precise value for the diffusion coefficients. This procedure was previously described by Walrand (1986).

3.4. *Preparation of γ-crystallins*

γ-Crystallins were prepared following the method described in Tardieu *et al.* (1992). The γ-crystallins used with all three techniques were the total γ-crystallin fraction extracted from the nuclei of fresh calf lenses. Although precluding solubility experiments in parallel, the choice of the total γ-crystallin fraction was imposed by the need to have enough material in one preparation for performing the three series of experiments. Nuclei were homogeneized in 4 volumes of physiological buffer [phosphate buffer pH 6.8, ionic strength 150 m*M* adjusted with KCl, supplemented with NaN_3, EDTA and dithiothreitol (DTT)]. The solution was centrifuged 40 min at 10 000*g* at 277 K in a Beckman Avanti 30 centrifuge. γ-Crystallins were prepared from the clear supernatant fraction by gel filtration using a Sephacryl S300 column (volume 120 ml) eluted with the phosphate buffer at 277 K. The γ-crystallin fractions were concentrated by ultrafiltration (Amicon cell with YM 10 membranes) and dialysed against buffer 1: a 10 m*M* ionic strength Na_2HPO_4/KH_2PO_4 buffer, pH 7.0, supplemented with 4 m*M* DTT. Their purity (absence of higher molecular weight β-crystallins or of degradation products) was checked in buffer 1 on a Superdex S75 column using an FPLC (fast protein liquid chromatography) system, which verifies at the same time that the γ-crystallins are monomeric. Different sample solutions were prepared from this stock solution by adding HCl equivalents (HCl Eq, one HCl Eq corresponds to one mole of HCl for one mole of protein) to obtain various solutions of γ-crystallins at different protein concentrations and pH. The addition of 3, 5, 7, 10, 14 and 15 HCl Eq resulted in pH 6.5, 5.4, 5.0, 3.8, 3.3 and 3.2, respectively. γ-Crystallin concentrations were measured either by UV absorption at 280 nm using $\varepsilon^{0.1\%}_{1\text{cm}} = 2$ or with an Abbe refractometer using $n = 1.3342 + 0.185c$.

The OP, SAXS and QELS experiments presented here made use of the same batch of γ-crystallins. It was checked with SAXS that experiments performed in different runs with other protein batches at the same pH and concentration conditions displayed the same behavior (not shown). The range of protein concentrations was 2–18 mg ml^{-1} for OP experiments, 10–22 mg ml^{-1} for SAXS and 7–22 mg ml^{-1} for QELS. The OP experiments were performed at four different pH levels obtained by addition of 0, 5, 10 and 15 HCl Eq. The QELS experiments were performed at five different pH values obtained by addition of 0, 3, 7, 10 and 14 HCl Eq. Three of these series: 0, 7 and 14 HCl Eq were then used for the X-ray experiments. The samples were made in a 10 m*M* phosphate buffer since the crystallins are unstable in the absence of any salt, which allowed us to keep the screening of the interparticle interaction potentials as low as possible. Since the γ-crystallins have a tendency to dimerize, their oligomeric state was verified before and after the OP, SAXS and QELS experiments using the Superdex S75 column and the FPLC system. A few per cent of dimers (5–10%) were indeed found in the protein pool after the OP experiments.

4. Results

4.1. *Variation with pH of virial coefficients*

The osmotic pressure experiments are shown in Fig. 1. The OP first varies linearly with protein concentration and then a curvature is observed. At pH 7 the OP increase with protein concentration is slightly lower than what would be expected without interactions, *i.e.* the second virial coefficient is negative, indicative of attractive interactions. Upon addition of HCl, the behavior is reversed and the second virial coefficient becomes positive, indicative of repulsive interactions. The curvature is more and more pronounced as the pH is further decreased.

The virial coefficients can be directly obtained from a polynomial fit of the measurements as a function of protein concentration. Since the protein solutions were at low concentrations, we only considered up to the second virial coefficient, A_2 (or B_2) *i.e.*,

$$\Pi/RT = (1/M)c + A_2c^2. \qquad (11)$$

Different fits were attempted, second order or third order, with and without a constant term. Whatever the fit, for each curve the constant term was found to be close to

Table 1. *Interaction parameters obtained from osmotic pressure measurements, extrapolation of X-ray structure factors and light-scattering measurements for various pH levels*

K_S* interpolated from OP and SAXS, K_D* interpolated from QELS.

Eq HCl/pH	A_2/OP (mol cm^3 g^{-2})	A_2/SAXS (mol cm^3 g^{-2})	$K_S^* = -2B_2^*$ (cm^3 g^{-2}) ($\times 10^{19}$)	K_D/QELS (cm^3 g^{-2}) ($\times 10^{19}$)	K_D^* (cm^3 g^{-2}) ($\times 10^{19}$)	$K_H = K_S^* + K_D$ (cm^3 g^{-1}) ($\times 10^{19}$)
0/7.0	-4.2×10^{-5}	-4.2×10^{-4}	3.3	−3.5	−4.3	−1
3/6.5			1.2	−3.6	−1.7	−0.5
5/5.4	1.6×10^{-4}		−1.3		0.2	−1.1
7/5.0		8.8×10^{-5}	−4.3	3.5	2.4	−1.9
10/3.8	1.0×10^{-3}		−10.4	6.2	5.8	−4.6
14/3.3		1.5×10^{-3}	−21.0	10.5	10.7	−9.3
15/3.2	1.9×10^{-3}		−23.9		11.8*	−12.1*

zero, the first virial coefficient close to the same M value and the A_2 values similar yet with a larger dispersion. The fits shown in Fig. 1, and the values given in Table 1, assume that the constant term is equal to zero and that the first virial coefficient, *i.e.* the molecular weight, is the same whatever the pH and is equal to the average of the determinations made for each curve independently, *i.e.* 25 kDa ± 2.5. This value is consistent with the presence of essentially monomeric γ-crystallins in solution yet a small amount of dimers were detected with FPLC after the OP experiment. The whole series demonstrates that the γ-crystallin interactions change from slightly positive to rather repulsive with decreasing pH.

4.2. *pH and protein concentration effects on the X-ray scattering curves*

The SAXS curves recorded at three different protein concentrations and three different pH values are shown in Figs. 2(*a*)–2(*c*). At pH 7, close to the isoelectric point, the intensity near the origin is higher than would be expected without interactions. Then, the normalized intensity near the origin decreases with the pH. The decrease is indicative of increasingly repulsive interactions when the solution becomes more acidic, in agreement with the γ-crystallins being more and more charged as the pH decreases. Experimental structure factors, calculated according to (4), and their best fits, determined as indicated in the theoretical part, are shown in Figs. 3(*a*)–3(*c*). As can be seen in the figures, the interaction model described in the theoretical part, which depends upon two parameters, the Hamaker constant and the charge, reproduces quite well the changes in curvature near the origin of the scattering curves as a function of pH. The Hamaker constant was first determined from a fit of the curves recorded at pH 7, *i.e.* at the isoelectric point. The values necessary to fit the curves were found to vary with concentration from 3.35 to 3.15 kT, close to the value calculated according to Israelachvili (1994) for a van der Waals potential (2.86 kT), and close to the Hamaker constant found to account for the γ-crystallin phase separation (2.7 kT) at 120 mg ml^{-1} (Malfois *et al.*, 1996).

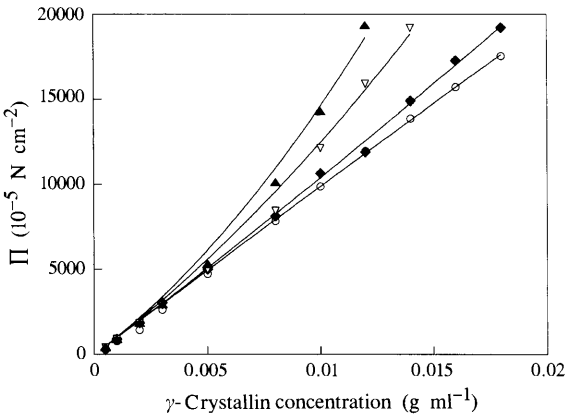

Fig. 1. OP measurements as a function of protein concentration for different pH: ○ pH 7.0, ♦ pH 5.4, ▽ pH 3.8 and ▲ pH 3.2. The best fits indicated in the figure are second-order fits with the constant term equal to zero and the first-order term bound to remain constant for the four series of experiments.

At lower pH, the best fit particle charge increases, as expected, with decreasing pH up to 6 charges at pH 3.3. The discrepancy with the number of charges calculated from the sequence, about 20 at pH 3.3, shows that the meaning of the best fit charge is not straightforward. The result might indicate either counterion condensation or variations of the attractive component with pH, neglected in the present study. Work is in progress to clarify the point. In any case and whatever the exact molecular meaning of the parameters involved, accounting for a concentration and pH series with only two parameters, Hamaker constant and effective charge, is already a success.

The X-ray structure factor at the origin is related to the osmotic pressure by,

$$S(c, 0) = (RT/M)(\partial\Pi/\partial c)^{-1}. \quad (12)$$

Therefore, if we stop at the second virial coefficient, we obtain,

$$1/S(c, 0) = 1 + (2M A_2)c. \quad (13)$$

Since the structure factor at the origin cannot be experimentally recorded, the best fit structure factors at the origin, $S_{calc}(c,0)$, were used instead. The A_2 values calculated from (13) are given in Table 1. As can be seen in the table, the SAXS values are consistent with

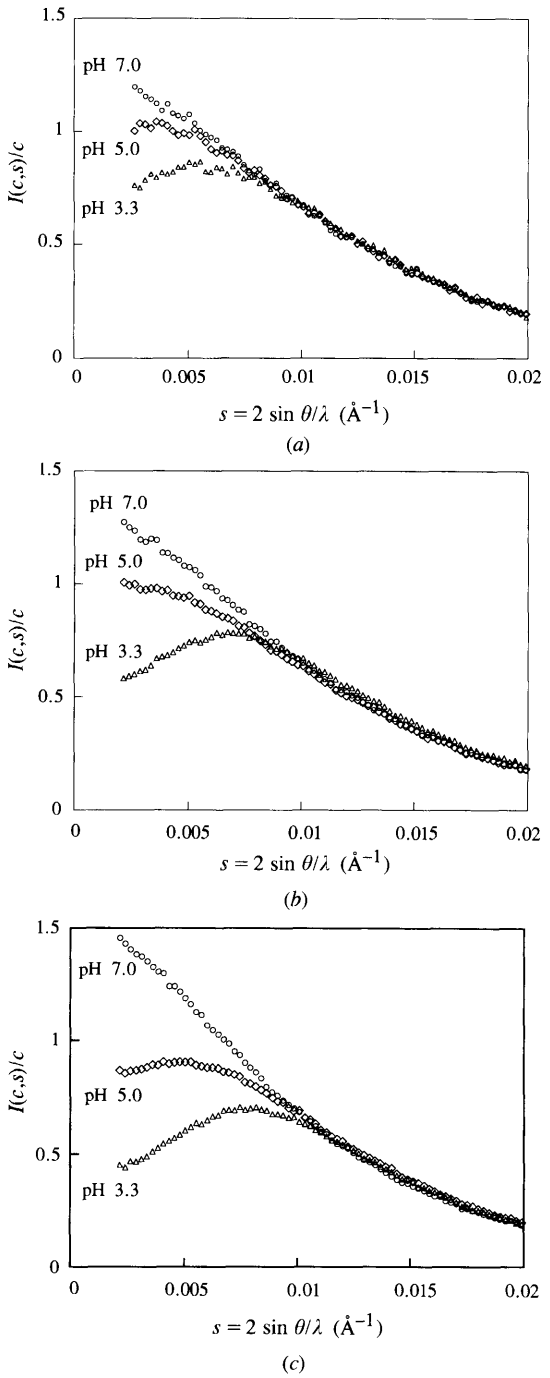

Fig. 2. SAXS measurements as a function of pH: ○ pH 7.0, ◇ pH 5.0, △ pH 3.3. (note that the batches are the same as those used for OP and QELS). (*a*), (*b*) and (*c*) are the experimental scattered intensities at different concentrations: (*a*) 10, (*b*) 14 and (*c*) 22 mg ml^{-1}).

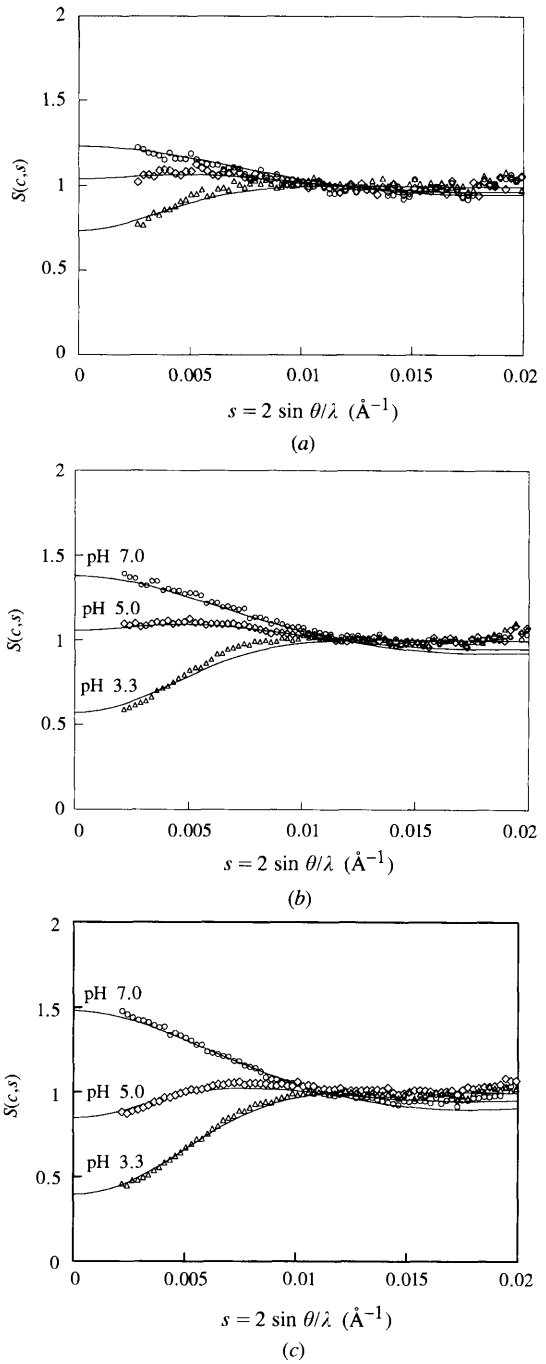

Fig. 3. Experimental and theoretical structure factors at different concentrations, (*a*, 10 mg ml^{-1}; *b*, 14 mg ml^{-1}; *c*, 22 mg ml^{-1}) as a function of pH: ○ pH 7.0, ◇ pH 5.0, △ pH 3.3. The theoretical structure factors (continuous lines) are calculated with a hard core of 36 Å in diameter; the attractive potential has a range equal to 3 Å and a depth corresponding to a Hamaker constant varying from 3.35 (*a–b*) to 3.15*kT* (*c*); the additional repulsive potential at pH 5.0 (◇) and pH 3.3 (△), has a range equal to the Debye length and depth varying with the electronic charge; *Z* varies from 2 (*a–b*) to 2.7 (*c*) at pH 5.0; *Z* varies from 4.5 (*a*) to 6 (*b–c*) at pH 3.3. The fits deviate at high angles since the model assumes perfect spheres and the proteins are only globular.

the OP values in the whole range of pH values analyzed: A_2 changes its sign close to the isoelectric point and increases with decreasing pH to reach similar values at low pH.

4.3. *Separation of static and dynamic coefficients*

The QELS experiments are shown in Fig. 4. The slope of the diffusion coefficient as a function of protein concentration at different pH varied from negative to positive values when more than 3 HCl Eq were added. (9) can be simplified, using a first-order expansion, to give,

$$\begin{aligned} D_m &= D_0(1 + K_D\rho_n) \\ &= D_0[1 + K_D(N_A/M)c], \qquad (14) \\ \text{with} \quad K_D &= K_H - K_S \end{aligned}$$

where K_S ($cm^3\ mol^{-1}$) is the static term equal to $-2B_2$ (2) and K_H is the hydrodynamic term which for hard spheres is nearly equal to 3/4 K_S. The role of K_D is, therefore, similar to the role of the second virial coefficient in an osmotic pressure experiment. With attractive interactions K_D is expected to be negative. With repulsive interactions K_D is positive. The error in the determination of D_m observed at 14 Eq HCl was found to be larger than in the other conditions and comparable to a previous observation of Neal (Neal, Purich & Cannel, 1984). The authors reported that in the case of solutions at low ionic strength and highly charged particles, the accuracy of the D_m determination was dropped. For γ-crystallins, the same observation was made when the HCl added was varied from 0 to 14 Eq.

Using (14), the QELS data were fitted by straight lines to get D_0 and K_D assuming that the D_0 value was the same whatever the pH, as shown in Fig. 4. This average D_0 value of $9.1 \times 10^{-7}\ cm^2\ s^{-1}$ corresponds to a hydrodynamic radius of 24.1 Å, which itself corresponds to the monomer size.

For the sake of comparison, K_D measured by QELS and K_S *i.e.* $-2B_2$ measured by OP and/or SAXS were plotted in Fig. 5. As can be seen in the figure, K_D varies linearly as a function of pH in the experimental pH range, whereas K_S is better fitted with a second-order polynomial approximation. The two sets of fits (K_D and K_S) were then combined to calculate the hydrodynamic term K_H as a function of pH. The K_H values are given in Table 1 and plotted in Fig. 5. K_H is always negative and remains close to zero until pH 5.0. In the case of hard spheres, K_S is expected to be equal to $-8V_p$ where V_p is the particle volume (*i.e.* $K_S = -2 \times 10^{-19}\ cm^3\ mol^{-1}$, $A_2 = 1.5 \times 10^{-4}\ mol\ cm^3\ g^{-2}$) and K_H is expected to be of the order of $0.75K_S$. Such an order of magnitude is observed close to 7 Eq HCl. When the interactions become more and more repulsive, K_H starts varying rapidly to reach values of the order of $0.5K_S$.

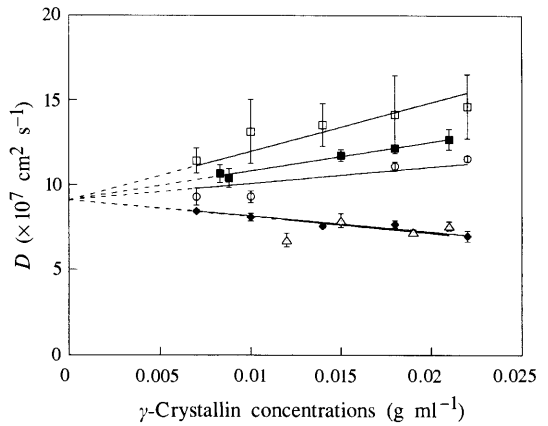

Fig. 4. QELS experiments as a function of protein concentration for various values of pH: ♦ pH 7.0, △ pH 6.5, ○ pH 5.0, ■ pH 3.8 and □ pH 3.3. The best fits indicated in the figures are those corresponding to the same D_0 values for all series of experiments. Note that the error bars increase when the interactions become more and more repulsive.

5. Discussion

The present study confirms that the type of interaction potentials, either attractive or repulsive, can be easily demonstrated by any of the three techniques. The variation of the second virial coefficients measured by OP or SAXS as a function of pH were in good quantitative agreement. The small remaining differences might originate from the data analysis itself: when the interaction potentials become stronger, more virial coefficients have a role to play and fitting the experimental data up to only the second virial coefficient is certainly a rough approximation. If K_D measured by QELS is taken as a quantitative measure of the second virial coefficient, the approximation may be more or less valid according to the type of interactions present in solution. The observation that the hydrodynamic term varies with the type of interactions, coming close to zero in attractive

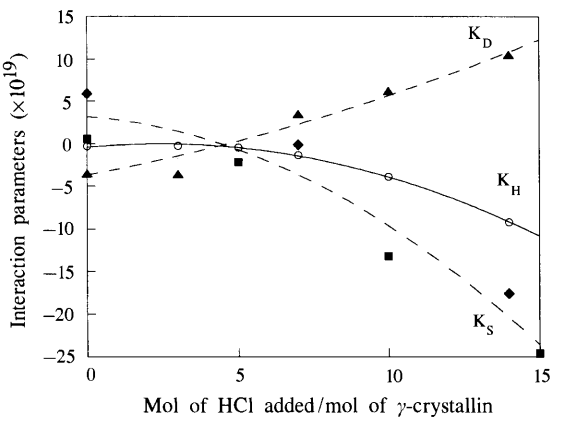

Fig. 5. Interaction parameters. $-2B_2$ measured by OP (■) and by SAXS (♦); K_D measured by QELS (▲). The solid line (○) is the locus of K_D ++ K_S and the other lines are to guide the eye.

conditions, is in agreement with the recent study of Muschol & Rosenberger (1995).

The general validity of the observation, however, remains to be established. Whatever the technique, the potential models able to account for a given value of the second virial coefficient are many. Since the SAXS curves are determined, not only by virial coefficients but also by the potential shape, the recording of complete X-ray scattering curves is a powerful tool to discriminate between different interaction models, to analyse whether only attractive or repulsive potentials play a part, or a combination of both. If the solution cannot be ascertained to be unique by any of the techniques, SAXS is potentially the most adequate to determine a minimum model (Haynes *et al.*, 1992; Eberstein *et al.*, 1994; Muschol & Rosenberger, 1995).

In terms of convenience, OP has the unique property that, since it is a way of counting particles, the lower the molecular weight, the better the accuracy or the smaller the amount of material and the concentration required. The lower limit of the particle molecular weight is, however, of the order of 10 000 because of the pore size of the membranes available. Once calibrated, the osmometer is fairly easy to use and quite rapid since experiments on one pH series can be carried out in a day. When the salt concentration is increased, the system is more and more difficult to equilibrate and we have not yet recorded reliable results beyond 500 m*M* salt. The range of osmotic pressure accessible, up to 2×10^{-1} N cm^{-2}, may also be a limitation, since with this equipment the range of accessible interactions is a function of the particle molecular weight. Osmotic stress experiments (Parsegian *et al.*, 1986) may sometimes compete advantageously with membrane osmometers.

When SAXS can be used, it appears once again as a convenient and versatile tool to study interactions in solutions of macromolecules (Ducruix *et al.*, 1996). Of course, when only the second virial coefficient (*i.e.* the structure factor at the origin) is needed, SAXS appears to be quite complicated approach compared with the simplicity and efficiency of OP. Static light scattering, which was not considered here, is also easier to use than X-rays when only the structure factor at the origin is needed (Muschol & Rosenberger, 1995). In terms of protein quantities, the amounts required are now comparable between the three techniques. The limitations here, of course, are the availability of a synchrotron radiation facility, of a small-angle camera at this facility, and of a set of programs to calculate theoretical curves.

QELS is rapidly becoming widespread as a diagnostic tool of the conditions that could lead to macromolecular crystallization. Following previous studies (Skouri *et al.*, 1992; Eberstein *et al.*, 1994; Veesler *et al.*, 1994; Muschol & Rosenberger, 1995; Lafont *et al.*, 1997), the present one confirms that indeed, QELS is a good tool to determine the sign of the second virial coefficient and, therefore, the type of interactions present in solution. From the value of the slope of the concentration dependence of the diffusion coefficient, the value of this coefficient cannot, however, be inferred since the hydrodynamic contribution plays an important role. The optimal range of molecular weight and protein concentration is complementary to those of OP since the lower the molecular weight the higher the concentration required. These optimal conditions are shared with SAXS. The major advantage of QELS compared with SAXS or OP is that it is able to conveniently assess the monodispersity as well as the polydispersity of the solutions, and to be sensitive to very high molecular weight species, that cannot be detected with the other techniques.

As far as γ-crystallins are concerned, the experiments presented here demonstrate that their behaviour in solution, as a function of pH, may be accounted for by the interplay of a short-range van der Waals attractive potential and a longer range coulombic repulsive potential. At acidic pH, the second virial coefficient can reach values at least one order of magnitude higher than would be expected from the simple case of hard spheres. Since the lens function is determined by the lens crystallin interactions, it is interesting to specify the parameters which may act on the interactions.

As far as proteins are concerned, the results obtained indicate that protein solutions of about 5–20 mg ml^{-1}, when studied at low ionic strength, may be far from ideal. As expected, the departure from ideality is all the more pronouced far from the isoelectric point. Such large interaction effects at low protein concentration might have undesirable consequences like precluding any accurate determination of radii of gyration. Since the problem has not yet, to our knowledge, been reported in the literature, other experiments are required to determine whether such strong interactions are only observed with small proteins, or are owing to some particular feature of γ-crystallins. Another explanation could be that, fortunately for us, most proteins have been studied so far in higher ionic strength buffers, in conditions where the charges are essentially screened.

It seems now widely accepted that solution studies may help to optimize crystallization conditions. The present study demonstrates that, in addition to the widely used light-scattering techniques, osmotic pressure and small-angle X-ray scattering are powerful tools to analyze the protein interactions at the basis of protein crystallization. The minimum potential model able to account for the low ionic strength phase diagram and for the shape of the X-ray curves was a combination of an attractive van der Waals potential and of a repulsive coulombic potential. These two potentials are expected to be the basic non-specific potentials acting in solutions with all small compact globular proteins. Other more specific effects like those associated with the salting-out process can only act on that basis.

6. Conclusions

Osmotic pressure, small-angle X-ray scattering and quasi-elastic light scattering have been used to study γ-crystallin interactions as a function of pH. The main results are summarized below.

At low ionic strength the interactions could be measured at low protein concentration. They were shown to vary from attractive to repulsive when going from the isoelectric point to more acidic pH. This seems to be a general observation for small compact proteins.

Osmotic pressure and small-angle X-ray scattering were both demonstrated to be convenient to establish interaction phase diagrams and measure second virial coefficients.

The pH (and temperature) phase diagram could be accounted for by the combination of an attractive van der Waals potential and of a repulsive coulombic potential. Such a combination should be of general validity for small compact proteins. More specific effects involved in protein crystallization can only act by modification of, and/or by additions to these fundamental interactions.

We can expect, in future, to predict solubility curves and phase diagrams from the type of experiments presented here.

We gratefully acknowledge CNRS (GdR 1092), CNES and the European CHM network 'Eye Lens Crystallins' for both financial support and exciting scientific discussions. We thank the technical staff at LURE for running the synchrotron machine. We thank Linda Sperling for critical reading of the manuscript and Patrice Vachette for stimulating comments during the experiments at LURE.

References

Belloni, L. (1991). *Neutron, X-ray and Light Scattering*, edited by P. Lindner & Th. Zemb, pp. 135–155. Amsterdam: Elsevier.

Belloni, L. (1993). *J. Chem. Phys.* **98**, 8080–8095.

Delaye, M. & Tardieu, A. (1983). *Nature (London)*, **302**, 415–417.

Depautex, C., Desvignes, C., Feder P., Lemonnier, M., Bosshard, R., Leboucher, P., Dageaux, D., Benoit, J. P. & Vachette, P. (1987). LURE: Rapport d'activit pour la priode Août 1985–1987, edited by Documentation CEN Saclay, 87.

Ducruix, A., Guilloteau, J. P., Riès-Kautt, M. & Tardieu, A. (1996). *J. Cryst. Growth.* **168**, 28–39.

Eberstein, W., Georgalis, Y. & Saenger, W. (1994). *J. Cryst. Growth* **143**, 71–78.

Eisenberg, H. (1976). *Biological Macromolecules and Polyelectrolytes in Solution*. Oxford: Clarendon Press.

Georgalis, Y., Zouni, A. & Saenger, W. (1992). *J. Cryst. Growth*, **18**, 360–364.

George, A. & Wilson, W. W. (1994). *Acta Cryst.* D**50**, 361–365.

Guinier, A. & Fournet, G. (1955). *Small-Angle Scattering of X-rays*. New York: John Wiley.

Hansen, J. P. & McDonald, I. A. (1986). *Theory of Simple Liquids*. New York: Academic Press.

Haynes, C. A., Tamura, K., Korfer, H. R., Blanch, H. W. & Prausnitz, J. M. (1992). *J. Phys. Chem.* **96**, 905–912.

Israelachvili, J. (1994). *Intermolecular and Surface Forces*. New York: Academic Press.

Kam, Z., Shore, H. B. & Feher, G. (1978). *J. Mol. Biol.* **123**, 539–555.

Koppel, D. E. (1972). *J. Chem. Phys.* **57**, 4814–4820.

Lafont, S., Veesler, S., Astier, J. P. & Boistelle, R. (1997). *J. Cryst. Growth.* In the press.

Lomakin, A., Asherie, N. & Benedek J. B. (1996). *J. Chem. Phys.* **104**, 1646–1656.

Luzzati, V. & Tardieu, A. (1980). *Annu. Rev. Biophys. Bioeng.* **9**, 1–29.

Malfois, M. (1995). PhD thesis, Université Paris-Sud, France.

Malfois, M., Bonneté, F., Belloni, L. & Tardieu, A. (1996). *J. Chem. Phys.* **105**, 3292–3300.

Malkin, A. J. & McPherson, A. (1994). *Acta Cryst.* D**50**, 385–395.

Mikol, V., Hirsch, E. & Giegé, R. (1990). *J. Mol. Biol.* **213**, 187–195.

Muschol, M. & Rosenberger, F. (1995). *J. Chem. Phys.* **103**, 10424–10432.

Neal, D. G., Purich, D. & Cannel, D. S. (1984). *J. Chem. Phys.* **80**, 3469–3477.

Parsegian, V. A., Rand, R. P. Fuller, N. L. & Rau, D. C. (1986). *Methods Enzymol.* **127**, 400–416.

Pecora, R. (1985). *Dynamic Light Scattering. Applications of Photon Correlation Spectroscopy*. New York/London: Plenum Press.

Skouri, M., Munch, J. P., Lorber, B., Giegé, R. & Candau, S. (1992). *J. Cryst. Growth*, **122**, 14–20.

Taratuta, V. G., Holschbach, A., Thurston, G. M., Blankschtein, D. & Benedek, G. B. (1990). *J. Phys. Chem.* **94**, 2140–2144.

Tardieu, A. (1994). *Neutron and Synchrotron Radiation for Condensed Matter studies*, Vol. III, edited by J. Baruchel, J. L. Hodeau, M. S. Lehmann, J. R. Regnard & C. Schlenker, pp. 145–160. Les Editions de Physique. Les Ulis: Springer-Verlag.

Tardieu, A. & Delaye, M. (1988). *Annu. Rev. Biophys. Biophys. Chem.* **17**, 47–70.

Tardieu, A., Vérétout, F., Krop, B. & Slingsby, C. (1992). *Eur. Biophys. J.* **21**, 1–12.

Thomson, J. A., Schurtenberger, P., Thurston, G. M. & Benedek, G. B. (1987). *Proc. Natl Acad. Sci. USA*, **84**, 7079–7083.

Veesler, S., Lafont S., Marcq, S., Astier, J. P. & Boistelle, R. (1996). *J. Cryst. Growth*, **168**, 124–129

Veesler, S., Marcq, S., Lafont S., Astier, J. P. & Boistelle, R. (1994). *Acta Cryst.* D**50**, 355–360.

Vérétout, F., Delaye, M. & Tardieu, A. (1989). *J. Mol. Biol.* **205**, 713–728.

Vérétout, F. & Tardieu, A. (1989). *Eur. Biophys. J.* **17**, 61–68.

Walrand, S. (1986). PhD thesis, Université Paris VII, France.

White, H. E., Driessen, H. P., Slingsby, C., Moss D. S. & Lindley P. F. (1989). *J. Mol. Biol.* **207**, 217–235.

Wistow, G. Turnell, B., Summers, L., Slingsby, C., Moss, D., Miller, L., Lindley, P. & Blundell, T. (1983). *J. Mol. Biol.* **170**, 175–202.

Zulauf, M. & D'arcy, A. (1992). *J. Cryst. Growth*, **122**, 102–106.